Dynamical Structure, Bonding, and Thermodynamics of the Superionic Sublattice in α-AgI

Brandon C. Wood and Nicola Marzari

Department of Materials Science and Engineering, Massachusetts Institute of Technology, Cambridge, Massachusetts 02139, USA

(Received 22 February 2006; published 17 October 2006)

We characterize the superionic phase transition and the lattice and electronic structures of the archetypal type-I superionic conductor α-AgI using extensive first-principles molecular dynamics calculations. We find that superionicity is signaled by a phase transition of the silver ions alone. In the superionic phase, the first silver shell surrounding an iodine displays a distinct dynamical structure that would escape a time-averaged characterization, and we capture this structure in a set of ordering rules. The electronic structure demonstrates a unique chemical signature of the weakest-bound silver in the first shell, which in turn is most likely to diffuse. Silver diffusion decreases upon melting, pointing to an unusual entropic contribution to the stability of the superionic phase.

DOI: 10.1103/PhysRevLett.97.166401 PACS numbers: 71.15.Pd, 66.30.Dn

Key advances in energy research have prompted a surge of interest in superionic materials as a crucial enabling technology for a variety of nanotechnological devices, including sensors, switches, batteries, and fuel cells. Of the superionics, AgI and related silver halides and sulfides have attracted particular attention because of the unusually high levels of ionic conductivity they exhibit, and as such are finding increased and varied technological implementation [1–4]. At normal pressure, AgI enters its superionic α phase above $T_c = 420$ K, at which temperature a phase transition to a body-centered cubic structure is accompanied by an increase in the silver conductivity of about 3 orders of magnitude [5]. Previous molecular dynamics studies using classical pair potentials have successfully reproduced experimental characteristics of the α and β phases, as well as the $\alpha \rightarrow \beta$ transition [6–11], but these are unable to describe the electronic structure in a dynamic environment, or to capture the phenomenology of the melting transition. In this regard, first-principles simulations provide unique and unbiased predictive power.

We performed Car-Parrinello molecular dynamics simulations [12,13] in the canonical ensemble at temperatures ranging from 200 to 1225 K. Each simulation ran for 50 ps following 5 ps of equilibration and was carried out in a 54-atom supercell, except the Wannier function calculations, which were performed in a 32-atom cell. Simulations used a plane-wave basis, the Perdew-Burke-Ernzerhof recipe for the exchange-correlation functional [14], $4d^{10}5s^1$ ultrasoft silver and $5s^25p^5$ norm-conserving iodine pseudopotentials [15,16], and cutoffs of 22 and 176 Ry for the wave functions and charge density, respectively. The fictitious CP mass was $\mu = 700$, with $\Delta t = 20$ au for $T \leq 950$ K, 15 au for 1100 K, and 10 au for 1225 K; and a Nosé-Hoover thermostat controlled the temperature [17]. The lattice parameter was fixed to be the experimental a_0 at T_m, motivated in part by the difficulty in determining an equilibrium volume and ionic ground state configuration for a soft and inherently disordered material [18].

First, we find evidence of a phase transition of the silver ions near the experimental T_c that is independent of the conformation and dynamics of the iodine sublattice and signals the transition into the superionic α phase. The silvers exhibit a sharp decrease in their diffusion behavior upon cooling below T_c, even though cubic boundary conditions forbid the iodine structural transition to the hexagonal wurtzite β phase. Results from simulations in which we immobilized the iodines in a fixed bcc configuration provide a secondary, stronger indicator of the independence of the silver transition from any iodine dynamics. Figure 1 shows the silver self-diffusion coefficients D_{Ag} for the fixed-iodine case and for a fully mobile lattice, as derived from the mean-square displacements (MSDs) via the Einstein relation, $D = \lim_{t\to\infty} \frac{1}{6t}\langle \mathrm{MSD}(t)\rangle$. In both cases, the slope of an Arrhenius plot of D_{Ag} shows a characteristic discontinuity near the experimental T_c. Immobilizing the iodine sublattice does lead to an overall

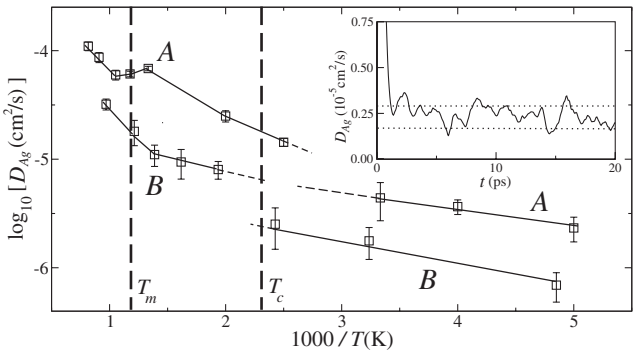

FIG. 1. Arrhenius plot of D_{Ag} for the fully mobile system (A) and with the iodine sublattice fixed (B), as obtained from the MSD. Experimental values for T_c and T_m at 1 atm are indicated. The inset shows the convergence of D_{Ag} for (A) at 200 K, as obtained by integrating the velocity autocorrelation function. Error bounds in the main graph represent twice the standard error and are shown as dotted lines in the inset to illustrate the agreement between the two methods.

decrease in D_{Ag}, suggesting local lattice fluctuations beneficial for silver mobility are frozen out, but the system retains its superionic behavior. Also of note in Fig. 1 is the unusual decrease of the silver ion diffusion coefficient upon melting at about 850 K, a tendency that has also been observed experimentally [5,19] but is not captured by classical potentials. The thermodynamic implication gives valuable insight into the stability of the superionic phase. The decreased mobility of the silver ions upon melting signals a decrease in the silver entropic contribution, meaning the iodines crystallize into the superionic state below T_m to increase the entropy of the silvers. Accordingly, the superionic phase acts as an intermediate between a pure solid and a pure liquid, with a high-entropy liquid sublattice flowing through a low-energy solid matrix. An entropically driven stabilization of the α phase is also consistent with experimental results [20], which determine the entropy difference between superionic and liquid phases to be unusually small.

Although it is not possible to separate the total energy of the system into respective sublattice contributions, we can get a quantitative picture of the energetic fluctuations associated with each sublattice by instead integrating the forces on the ions, which are trivially lattice resolved. In particular, we have for the evolution of the sublattice-resolved energy $U|_0^t = \sum_i \int_{\tau=0}^{t} \mathbf{F}_i(\tau) \cdot \dot{\mathbf{r}}_i(\tau) d\tau$, where $t = 0$ represents some equilibrated reference configuration and the index i runs over all ions in the given sublattice. Since in the canonical ensemble, fluctuations σ in the total energy are related to the specific heat capacity C_V as $\sigma^2 = k_B T^2 C_V$, we can derive a heat capacitylike quantity $C_V^{(i)}$ that is sublattice resolved using the fluctuations in the evolution of the energy, as derived from the ionic forces. Robustness was verified by ensuring that the evolution of the total internal energy could be recovered to within numerical error by summing over all ions. Plots of $C_V^{(\mathrm{Ag})}$ and $C_V^{(\mathrm{I})}$ are shown in Fig. 2. In the silver-resolved $C_V^{(\mathrm{Ag})}$ plot, we observe clear dropoffs at 400 and 850 K, corresponding to T_c and T_m, respectively. Examination of the iodine-resolved $C_V^{(\mathrm{I})}$ curve, however, reveals no detectable dropoff near T_c (although the corresponding behavior at T_m is clearly visible). As in Fig. 1, we can thus link the superionic transition to the silver sublattice only.

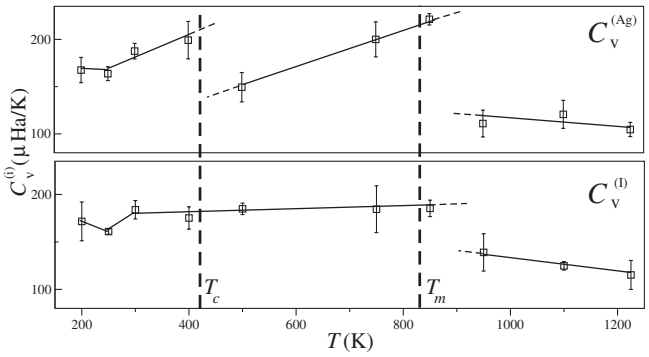

FIG. 2. Specific heat capacities for the silver and iodine sublattices (see text), with the experimental T_c and T_m indicated. Solid lines are intended as a guide for the eye.

We note that an order-disorder transition of the silver ions at T_c has been reported previously [21,22]. Symmetry arguments allow the 20-four bcc tetrahedral interstitial sites surrounding an iodine to be organized into six inequivalent sublattices [23], the occupancies of which can be tracked independently as a signal of the transition. Our results confirm an ordering tendency for the silvers below T_c, characterized by a splitting into higher- and lower-occupancy sublattices. The independent ordering tendency of the silver sublattice upon cooling is observable despite the inhibition of the $\alpha \rightarrow \beta$ transition, in agreement with Ref. [21]. However, at these low temperatures, more extensive statistical sampling is necessary to allow for comparison of the ordered phase with those proposed in the cited studies.

We have also investigated the most frequented pathways for the silver ions by tracking their positions with respect to the iodines and averaging the resulting trajectories. Figure 3 shows isosurface and slice plots for the silver ion density in the conventional cubic unit cell surrounding an iodine. Our results confirm that the highest-density regions lie near the tetrahedral sites, with silver ion density smeared toward the octahedral sites, in agreement with the experimental findings of Ref. [24].

Radial pair distribution functions offer additional insight into the preferred organization of the silver ions. The silver-silver function $g_{\mathrm{Ag\text{-}Ag}}(r)$ (Fig. 4) illustrates a zero probability of finding silver ions closer together than $R_{\mathrm{Ag\text{-}Ag}} = 2.4$ Å, which precludes simultaneous occupation of nearest-neighbor tetrahedral interstitial sites. Integration of $g_{\mathrm{Ag\text{-}I}}(r)$ over the first peak reveals that on average, each iodine has four nearest neighbors in the first coordination shell, consistent with geometric expectations for tetrahedral site occupancy. In addition, $g_{\mathrm{Ag\text{-}I}}(r)$ indicates the highest probability distance for silvers surround-

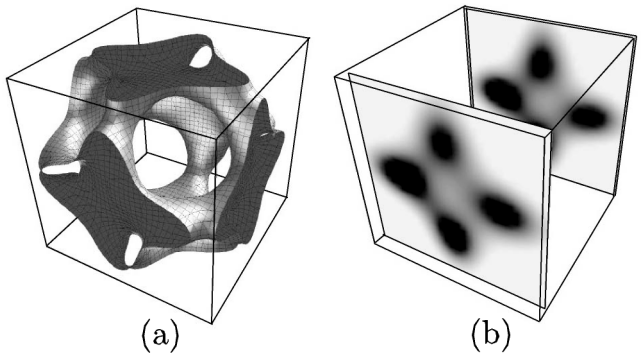

FIG. 3. (a) The isosurface of silver trajectories at 750 K in the conventional cubic unit cell surrounding an iodine. The eight nearest-neighbor iodines surrounding the iodine at the center are located at the vertices of the cube. (b) A slice plot of (a), revealing higher-density (darker) silver occupancy regions.

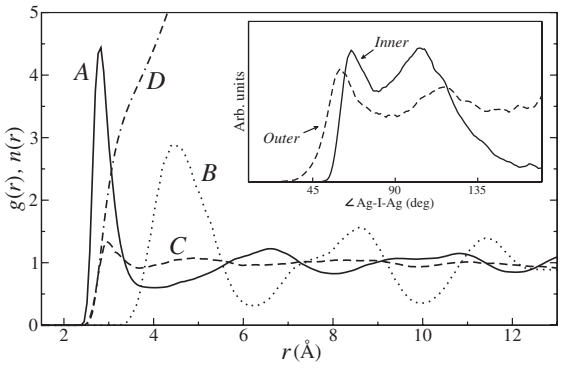

FIG. 4. Radial pair distribution functions for (*A*) Ag-I, (*B*) I-I, and (*C*) Ag-Ag, along with the integrated Ag-I $n(r)$ curve (*D*), at 750 K. The inset shows the angular distributions of the four silver ions in the first shell surrounding an iodine, measured with respect to the other silvers in the shell and resolved according to the three innermost silvers and the fourth outer silver.

ing an iodine is at $R_{\text{Ag-I}} = 2.6$ Å, corresponding to the distance to a tetrahedral site. However, a time-resolved analysis suggests a more detailed decomposition of the first peak of $g_{\text{Ag-I}}(r)$. We find that most commonly, three of the four nearest-neighbor silver ions simultaneously occupy a shell corresponding to the tetrahedral site distance (the number varies from 2.7 to 3.0 on average, with lower temperatures favoring higher values). The fourth silver is seen to transition regularly between this shell and its equivalent for a neighboring iodine such that on average, it fills a transition zone between the two, defined by $2.8 \lesssim R_{\text{Ag-I}} \lesssim 4.2$ Å. The transitioning rate is temperature dependent and disappears rapidly for $T < T_c$. The fourth silver also possesses an angular distribution distinct from its three inner counterparts, as indicated in the inset of Fig. 4. The Ag-I-Ag angles for the closest three silvers reveal preferences at 65° and 105°, and higher angles are uncommon. However, the angles introduced by the inclusion of the fourth nearest neighbor are comparatively diffuse and have significant probabilities towards larger values. This suggests that whereas the closest three silvers are clustered and correlated in their positions, the fourth silver is relatively unconstrained in its angular configuration and is affected only marginally by the orientations of the remaining three. Transitions of this unconstrained fourth silver between coordination shells represent the primary factor behind silver diffusion—an observation that would escape experimental investigations.

The above analysis allows for the definition of a set of ordering rules that govern the instantaneous distribution of silver ions in the first shell surrounding an iodine: (1) four silver ions populate the first shell; (2) no two silver ions occupy neighboring tetrahedral sites; (3) on average, three silver ions surround an iodine at a radius of $R_{\text{Ag-I}} = 2.6$ Å, the tetrahedral interstitial distance; (4) a fourth silver transitions between that shell and a second shell at $R_{\text{Ag-I}} \gtrsim 4.2$ Å, associated with a neighboring iodine, and the transition rate between the two is temperature dependent and disappears below T_c; (5) the angular positions of the three inner silvers are correlated, whereas the fourth (outer) silver is relatively unconstrained; and (6) silver ions tend to organize into high- and low-occupancy sublattices at temperatures below T_c.

We examined the maximally localized Wannier functions (MLWFs) to obtain a local picture of bonding in a dynamic environment [25]. Plotting the time-averaged radial distribution of the four iodine Wannier function centers (WFCs) about their parent ion reveals an unexpected bimodal separation into short-distance, highly localized WFCs and longer-distance, partially delocalized WFCs (Fig. 5). Further isolating Wannier functions associated with each of the two peaks and plotting the time- and statistical-averaged contours for the WFCs around the iodines yields the isosurfaces shown in the insets of Fig. 5. The long-distance Wannier centers (LWFCs) tend to align along the cubic axes toward the octahedral interstitial sites. Their orientations relate to the observed smearing of the silver occupancy from the electrostatically preferred tetrahedral sites towards the octahedral face centers and suggest that these orbitals correspond to directional interactions between silvers and iodines. However, short-distance iodine Wannier centers (SWFCs) exhibit a random angular distribution, as expected for a strictly Coulombic picture. Comparing the peak areas in Fig. 5 reveals that of the four WFCs surrounding an iodine, 30% on average can be classified as SWFCs, a figure which agrees with the likelihood for a first-shell silver to be found in the mobile transition zone. This value also correlates well with the experimental likelihood of a silver to be located outside the tetrahedral interstitial site [24,26], a quantity confirmed by our findings.

A detailed picture of the correlation between the delocalization extent of the iodine MLWFs and the positions of nearby silver atoms is offered in Fig. 6. There is clear evidence of a chemical interaction between LWFCs and silver atoms within a threshold radius of $R_{\text{Ag-I}} \lesssim 3.25$ Å and a solid bond angle of $|\theta| \lesssim 15°$, indicating that bond-

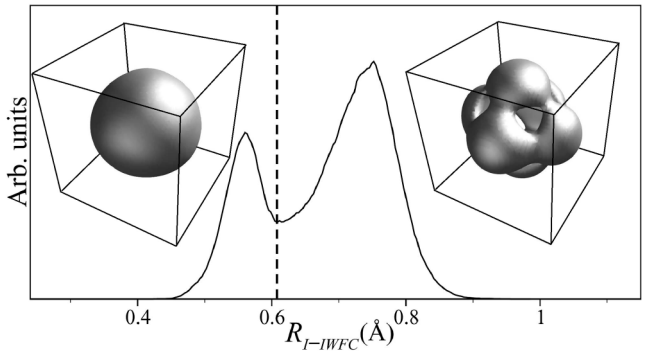

FIG. 5. Histogram of distances between iodine WFCs and iodine nuclei. The insets are contours of the iodine WFC distribution about their nuclei for WFCs on either side of the broken line.

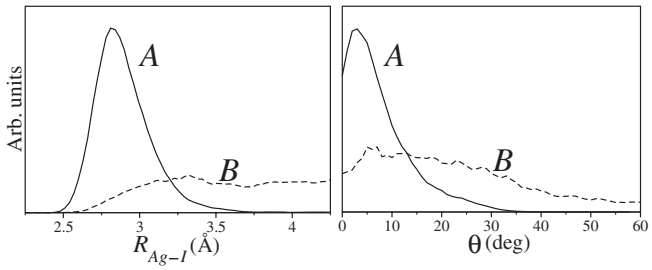

FIG. 6. Histograms of interionic bond distance and bond angle for the silvers closest to iodine WFCs, resolved into (*A*) long-distance and (*B*) short-distance Wannier functions. The bond angle θ is defined as the angle between $\mathbf{R}_{\text{Ag-I}}$ and $\mathbf{R}_{\text{IWFC-I}}$.

ing with LWFCs is highly directional. As a quantitative measure of these chemical interactions, we have calculated the Born effective charges for the ionic species using the electric-enthalpy method of Refs. [27]. Our values of $Z^* = \pm 1.22$ are larger than the integral values expected for a purely ionic crystal, further supporting our conclusions. Figure 6 shows no corresponding directionality for bonding with SWFCs, indicating these interactions can be attributed to weaker electrostatics. Moreover, examination of the radial distribution for first-shell silvers closest to SWFCs places them within the defined transition zone. We therefore conclude that silvers contributing to D_{Ag} are those which are not bound to LWFCs, meaning they are minimally constrained both radially and angularly. Most commonly, the outermost of the four first-shell silvers fills these criteria, as a lack of stronger directional interactions with LWFCs also increases the average Ag-I bond distance. This comparatively unconstrained, mobile fourth silver fleetingly occupies the transition zone until it is captured by a neighboring iodine, leading to net diffusion. At higher temperatures, thermal disordering breaks a greater number of bonds between silvers and LWFCs, promoting more nearby silvers into the transition zone. As such, the overall fraction of occupied tetrahedral sites decreases and diffusion is enhanced.

In conclusion, we have shown that the transition to the superionic α phase of AgI is signaled by an independent phase transition of the silver sublattice alone, characterized by a disordering of the silvers and a sharp increase in their diffusivity. Upon melting, D_{Ag} decreases, pointing to an unusual entropic contribution to the stabilization of the superionic phase. We have also identified diffusion pathways for superionic silver ions above T_c, and a time-resolved analysis of ion trajectories has allowed us to define a set of ordering rules that govern the instantaneous distribution of silvers in the first shell surrounding an iodine. Finally, we have found that of the four first-shell silvers, the closest three are strongly correlated and restricted in their angular distribution, and that they are involved in anisotropic, directional bonding to an iodine. The fourth silver is bound only weakly and is relatively unconstrained, and we have isolated it as the dominant contributor to diffusion.

Funding for this work has been provided by the DOE CSGF, and MURI Grant No. DAAD 19-03-1-0169. Calculations have been done with the Quantum-ESPRESSO package [28] using computational facilities provided through NSF Grant No. DMR-0414849. The authors also wish to thank Professor Bernhard Wuensch for helpful discussions.

[1] K. Terabe *et al.*, Nature (London) **433**, 47 (2005).
[2] M. Lee *et al.*, Appl. Phys. Lett. **85**, 3552 (2004).
[3] T. Minami, T. Saito, and M. Tatsumisago, Solid State Ionics **86–88**, 415 (1996).
[4] P. Boolchand and W. J. Bresser, Nature (London) **410**, 1070 (2001).
[5] A. Kvist and A. M. Josefson, Z. Naturforsch., A: Astrophys., Phys. Phys. Chem. **23**, 625 (1968).
[6] P. Vashishta and A. Rahman, Phys. Rev. Lett. **40**, 1337 (1978); M. Parrinello, A. Rahman, and P. Vashishta, Phys. Rev. Lett. **50**, 1073 (1983).
[7] F. Shimojo and M. Kobayashi, J. Phys. Soc. Jpn. **60**, 3725 (1991).
[8] K. O'Sullivan, G. Chiarotti, and P. A. Madden, Phys. Rev. B **43**, 13 536 (1991).
[9] F. Zimmer *et al.*, J. Chem. Phys. **112**, 6416 (2000).
[10] J. L. Tallon, Phys. Rev. B **38**, 9069 (1988).
[11] For reviews on the subject, see S. Hull, Rep. Prog. Phys. **67**, 1233 (2004); D. A. Keen, J. Phys. Condens. Matter **14**, R819 (2002).
[12] R. Car and M. Parrinello, Phys. Rev. Lett. **55**, 2471 (1985).
[13] K. Laasonen *et al.*, Phys. Rev. B **47**, 10 142 (1993).
[14] J. P. Perdew, K. Burke, and M. Ernzerhof, Phys. Rev. Lett. **77**, 3865 (1996).
[15] N. Troullier and J. L. Martins, Phys. Rev. B **43**, 1993 (1991).
[16] D. Vanderbilt, Phys. Rev. B **41**, 7892 (1990).
[17] S. Nosé, J. Chem. Phys. **81**, 511 (1984); Mol. Phys. **52**, 255 (1984); W. G. Hoover, Phys. Rev. A **31**, 1695 (1985).
[18] Varying the supercell volume by up to 8% in test runs had no measurable effect on the diffusive properties.
[19] H. Araki, T. Koishi, and S. Tamaki, J. Phys. Soc. Jpn. **68**, 134 (1999).
[20] W. Biermann and W. Jost, Z. Phys. Chem. (Frankfurt/Main) **17**, 139 (1960).
[21] P. A. Madden, K. F. O'Sullivan, and G. Chiarotti, Phys. Rev. B **45**, 10 206 (1992).
[22] C. Seok and D. W. Oxtoby, Phys. Rev. B **56**, 11 485 (1997); Phys. Rev. B **58**, 5146 (1998).
[23] G. Szabó, J. Phys. C **19**, 3775 (1986).
[24] R. J. Cava, F. Reidinger, and B. J. Wuensch, Solid State Commun. **24**, 411 (1977).
[25] N. Marzari and D. Vanderbilt, Phys. Rev. B **56**, 12 847 (1997).
[26] V. M. Nield *et al.*, Solid State Ionics **66**, 247 (1993).
[27] P. Umari and A. Pasquarello, Phys. Rev. Lett. **89**, 157602 (2002); I. Souza, J. Íñiguez, and D. Vanderbilt, Phys. Rev. Lett. **89**, 117602 (2002).
[28] S. Baroni *et al.*, URL http://www.quantum-espresso.org/.